atmosphere

MDPI

Article

Prediction of Transient NO_x Emission from Diesel Vehicles Based on Deep-Learning Differentiation Model with Double Noise Reduction

Jiaqiang Li [1,2], Yang Yu [1,2,3], Yanyan Wang [1,2], Longqing Zhao [1,2] and Chao He [1,2,*]

1 School of Machinery and Transportation, Southwest Forestry University, Kunming 650224, China; lijiaqiang@swfu.edu.cn (J.L.); yangyu1019@whut.edu.cn (Y.Y.); wangyy@swfu.edu.cn (Y.W.); mr@swfu.edu.cn (L.Z.)
2 Key Laboratory of Motor Vehicle Environmental Protection and Safety in Plateau Mountainous Areas of Yunnan Province, Kunming 650224, China
3 Hubei Key Laboratory of Advanced Technology Automotive Components, School of Automotive Engineering, Wuhan University of Technology, Wuhan 430070, China
* Correspondence: chao.he@swfu.edu.cn

Abstract: For diesel engines, accurate prediction of NO_x (Nitrogen Oxides) emission plays an essential role in virtual NO_x sensor development and engine design under situations of actual road driving. However, due to the randomness and uncertainty in the driving process of diesel vehicles, it is difficult to make predictions about NO_x emissions. In order to solve this problem, this paper proposes differential models for noise reductions of NO_x emissions in time series. First, according to the internal fluctuation of time series, use SSA (Singular Spectrum Analysis) to reduce the noises of the original time series; second, use ICEEMDAN (Improved Complete Ensemble Empirical Mode Decomposition with Adaptive Noise) to decompose the noise-reducing data into several relatively stable subsequences; third, use the sample entropy to calculate the complexity of each subsequence, and divide the sequences into high-frequency ones and low-frequency ones; finally, use GRU (Gated Recurrent Unit) to complete the prediction of high-frequency sequences and SVR (Support Vector Regression) for the prediction of low-frequency sequences. To obtain the final models, integrate the prediction results of the subsequences. Make comparisons with five single models, SSA single-processing models, and ICEEMDAN single-processing models. The experimental results show that the proposed model can predict the instantaneous NO_x emissions of diesel engines better than the single model and the model processed by SSA, and the differentiated model can effectively improve the execution speed of the model.

Keywords: diesel car; nitrogen oxide transient prediction; deep learning; signal processing

Citation: Li, J.; Yu, Y.; Wang, Y.; Zhao, L.; He, C. Prediction of Transient NO_x Emission from Diesel Vehicles Based on Deep-Learning Differentiation Model with Double Noise Reduction. *Atmosphere* **2021**, *12*, 1702. https://doi.org/10.3390/atmos12121702

Academic Editors: Sheng-Lun Lin and Xin Wang

Received: 24 November 2021
Accepted: 15 December 2021
Published: 20 December 2021

1. Introduction

The diesel vehicle is the main source of NO_x emission. In China, according to the 2019 China Mobile Source Environmental Management Annual Report, diesel vehicles account for 9.1% of motor vehicles in China, but the contribution rate of NO_x emission reaches 70% of the total vehicle emissions [1]. At the same time, China has implemented NO_x emission reduction regulations, which limit the NO_x emission of motor vehicles strictly, and put forward higher requirements for automobile manufacturers to adjust the engine component parameters. Traditionally, in order to reduce emissions by adjusting engine component parameters, it is necessary to go through the engine test bench or actual driving. It is very expensive and inefficient to evaluate the success of the adjustment process by means of PEMS (Portable Emission Measurement System). Therefore, in the actual road driving process, it is very important to understand the causal relationship between vehicle operating parameters and emissions and to establish relevant reliable models.

In recent years, some scholars have used the chassis dynamometer or the engine test bench to collect the engine working data and construct the models according to the data obtained in the steady-state. Table 1 presents the results of some recent studies on NO_x steady-state prediction by some authors.

These studies have achieved ideal experimental results, but the data obtained under steady-state conditions cannot capture the transient behavior of the engine from part load to full load as well as the hysteresis effect of the engine under start, stop, or cold start conditions [2], which is often quite different from the emission data generated by diesel vehicles driving on the real road.

Table 1. Some models for NO_x steady-state prediction.

Basic Model(s)	Preprocessing Method	Reference
Backpropagation neural network	Means of mutual information	[3]
Artificial Neural Network	Uncertainty analysis	[4]
Multi-layer perceptron	Non-dominated sorting genetic algorithm II	[5]
Support vector machine	Model parameters optimization	[6]
Long Short-Term Memory	Encoder-Decoder	[7]

In actual road driving, the NO_x emission data of the diesel engine is a highly nonlinear, complex, and changeable sequence. Coupled with the complexity of engine characteristics and the uncertainty of drivers in the actual road operation process, it is very difficult to construct a highly nonlinear equation group for NO_x emission modeling. Traditional modeling methods for NO_x transient emissions include physical or chemical as well as empirical or semi-empirical assumptions. For example, Maurya et al. [8] used the commercial 3D CFD (Computational Fluid Dynamics) engine simulation tool STAR-CD, combined with the mesh generator es-ice, to analyze the combustion process of a dual-fuel engine using a computational fluid dynamics (CFD) model, and derived the effect of EGR on the combustion and performance of the dual-fuel engine. Stelios A et al. [9] used a semi-empirical zero-dimensional two-zone model to predict NO_x variation with engine load/speed, fuel injection timing, EGR rate, boost pressure, and fuel injection pressure at a relatively low cost. CFD models based on physical chemistry are commonly used for NO_x predictions. By calculating the physical and chemical process of fuel combustion, NO_x emission can be estimated accurately. However, due to the complex structure, high computational cost, and long time required, CFD models cannot be applied in real time [10,11]. Based on physical and chemical properties and empirical assumptions, these methods are very difficult to model instantaneous NO_x emissions [12] and have limited performance in predicting NO_x emissions during actual road driving [13].

With the gradual rise of machine learning, as it is unnecessary to understand the complex physical and chemical knowledge behind the research object, any additional complexity will be incorporated into the models when having enough data. At the same time, the method can consider the impact of environmental conditions on emissions that are difficult to analyze by physical and chemical models [14], so it is widely used by scholars. Liu et al. [15] used the integrated method of PCA (Principal Component Analysis) and genetic algorithm to search for the best super parameters of support vector machine to predict the steady-state and transient NO_x emissions of diesel engines. Ideal results can be achieved by making predictions of the steady-state emission, but the results of transient emissions still have large errors at some operating points. Sáez et al. [16] used a single artificial neural network to predict the transient NO_x emission of diesel engines with input variables of vehicle speed and acceleration, engine speed and torque, intake temperature as well as air mass flow, which the best result of R^2 was only 0.82. In view of the characteristics of the NO_x transient emission time series of diesel vehicles, such as highly non-stationary, irregular fluctuation frequency as well as internal complexity and variability, as time goes on, the traditional machine learning algorithm may lose learning abilities [17]. Deep learning has better learning performance for the highly complex nonlinear data, showing

more excellent performance, but at present, few scholars use deep-learning methods to model transient NO_x emissions of diesel vehicles. Shin et al. [18] used the DNN (Deep Neural Network) and Bayesian optimization method to optimize the hyper-parameter and predict the NO_x transient emission, which improved the prediction accuracy and model stability significantly. However, compared with the single deep neural network, researchers found that signal processing can extract signal features effectively [19] and machine learning algorithms have been used in the field of wind speed prediction, power load forecasting, and financial field. For instance, Ma et al. [20] predicted wind speed using double decomposition, error correction strategies, and long- and short-term memory neural networks. Tong et al. [21] proposed a deep learning-based model that refines features from historical load data and associated temperature parameters by stacking denoised self-encoders and then training a support vector regression (SVR) model to predict the total load for the coming day. Niu et al. [22] used a combination of variational modal decomposition and LSTM to predict stock price changes with good predictive performance.

In this study, the vehicle exhaust online monitoring platform is used to obtain the NO_x emission data of two buses in the actual road driving process, and the in-depth learning model GRU (Gated Recurrent Unit) is used to establish the instantaneous NO_x emission model. Since there are noises in the collected data, SSA (Singular Spectrum Analysis) and ICEEMDAN (Improved Complete Ensemble Empirical Mode Decomposition with Adaptive Noise) are used to filter the noise in the data. Considering that the subsequences generated by the ICEEMDAN decomposition increase the computational cost, the SVR (Support Vector Regression) models of the differentiation models are used to replace the low-frequency subsequence GRU models.

2. Methodology

2.1. Singular Spectrum Analysis

SSA is a non-parametric method for studying nonlinear time series [23]. Based on time series, the SVD (Singular Value Decomposition) of the specific matrix is constructed. The specific algorithm process is as follows [24]:

Define the NO_x series data as $\{h_i, i = 1, 2, \ldots, N\}$ and then calculate the Hankel [25] trajectory matrix:

$$H = \begin{pmatrix} h_1\, h_2\, \ldots\, h_k \\ h_2\, h_3\, \ldots\, h_{k+1} \\ \vdots\, \vdots\, \cdots\, \vdots \\ h_L\, h_{L+1}\, \ldots\, h_N \end{pmatrix} \tag{1}$$

L represents the sliding window length parameter and $1 < L < N$, K is defined as $N - L + 1$. Matrix H is the trajectory matrix. The resulting trajectory matrix is then SVD (Singular Value Decomposed), where H can be rewritten as:

$$H = \sum_{i=1}^{d} H_i, \text{ with, } H_i = \sqrt{\lambda_i} U_i V_i^T \tag{2}$$

where $d = rank(H)$ and it is the number of intrinsic components or modes with non-zero intrinsic values. λ_i is the singular value in descending order. U_i and V_i are the related left and right singular vectors, respectively. The set denoted by $\left\{\sqrt{\lambda_i}, U_i, V_i\right\}$ is called the feature set. Then $H_i (i = 1, 2, 3, \cdots, d)$ in the trace matrix is decomposed into signal and noise. However, an important step is to identify the subset of features that contain the main variation of H. This is equivalent to approximating the matrix $\widetilde{H}$ by the combination of the first r elementary matrices using the following equation: $\widetilde{H} = \sum_{i=1}^{r} U_i \sqrt{\lambda_i} V_i^T$, $\widetilde{H}$ is attributed to the signal, r represents the number of features selected for signal reconstruction, and the residual $R = \sum_{i=r+1}^{d} U_i \sqrt{\lambda_i} V_i^T$ is treated as noise.

2.2. Improved Adaptive Noise Fully Integrated Empirical Mode Decomposition

In order to overcome the shortcomings of EEMD and CEEMDAN algorithms [26], Colominas et al. improved the CEEMDAN algorithm [27]. Different from the traditional method of adding Gaussian white noise, ICEEMDAN extracts the k-th IMF component through EMD decomposition of Gaussian white noise [28], calculates the local mean value of signal plus noise for each modal component, and defines the IMF obtained by decomposition as the difference between the residual signal and local mean.

First, define $\mathrm{M}(\cdot)$ as the local mean value of the signal, $E_k(\cdot)$ is the k-th mode component after EMD decomposition, then we have $E_1(x) = x - M(x)$, and the main steps are as follows:

The first IMF of the given white noise is added to the original sequence $X(t)$ as follows:

$$X^i = X + \beta_0 E_1\left(w^i\right) \tag{3}$$

where β_0 represents the noise standard deviation. w^i is the added white noise.

Find the local mean $M(.)$ of $X^i(t)$, calculate the average of the local mean and obtain the following residuals:

$$R_1 = \frac{1}{N}\sum_{i=1}^{N} M\left(X^i\right) \tag{4}$$

where N is the number of times to add noise.

Obtain the first IMF as follows:

$$IMF_1 = X - R_1 \tag{5}$$

For $k = 2, 3, \cdots, K$, the residual and the k-th IMF can be calculated by Formulas (6) and (7):

$$R_k = \frac{1}{N}\sum_{i=1}^{N} M\left(R_{k-1} + \varepsilon_{k-1} E_k\left(w^j\right)\right) \tag{6}$$

$$IMF_k = R_{k-1} - R_k \tag{7}$$

where ε is the ratio of the added noise.

2.3. Gated Recurrent Unit

Because of the gradient vanishing problem in traditional RNN networks [29], it is difficult to solve the long-term dependence problem in practical application, which makes RNN training very difficult. To solve this problem, LSTM and GRU use different functions to calculate the state of the hidden layer by adding "memory cell" structures into the hidden layer. The "memory cell" of LSTM is composed of three gates: input gates, forgetting gates, and output gates, while the GRU "memory cell" is only composed of update gates and reset gates, with fewer training parameters and faster calculations. The structure of the GUR neural network is shown in Figure 1 [29].

The function of the update gate is to control the state information of the previous time into the current state. The larger the value of the update gate is, the more state information will be brought into the previous moment. The formula of the update gate is [30]:

$$z_t = \sigma(W_r \times [h_{t-1}, x_t] + b_r) \tag{8}$$

where h_{t-1} contains the information of the previous node, x_t is the current input, σ is the activation function, w is the neuron connection weight, b is the neuron bias value.

The function of the reset gate is to control the forgetting degree of state information from the previous moment. When the reset gate is smaller, more state information is forgotten. The calculation formula of the reset gate is [31]:

$$r_t = \sigma(W_t \times [h_{t-1}, x_t] + b_z) \tag{9}$$

After obtaining the gating signal, the gating signal is reset to obtain the reset data, and then use *tanh* to activate the functions to obtain the candidate hidden state:

$$\widetilde{h}_t = tanh\left(W_{\widetilde{h}} \times [r_t \cdot h_{t-1}, x_t] + b_{\widetilde{h}}\right) \tag{10}$$

In the update phase, when the state information is changed, the update gate is used for controlling [32], then the hidden layer state at time t can be expressed as follows:

$$h_t = (1 - z_t) \cdot h_{t-1} + z_t \cdot \widetilde{h}_t \tag{11}$$

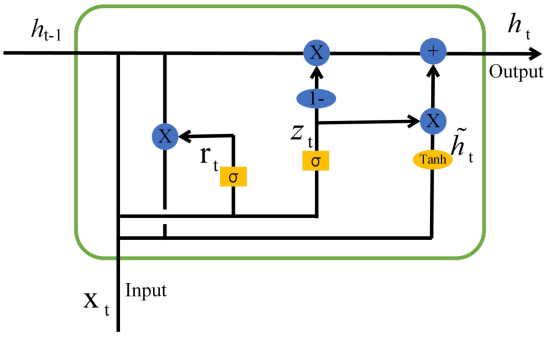

Figure 1. Structure of GRU.

2.4. Support Vector Regression

Support Vector Regression is a supervised learning algorithm for classification and regression, solved by feature mapping the input controls. With powerful theoretical concepts and applicable to nonlinear data fitting, SVR has been proven by a large number of scholars to outperform general neural networks [33] and machine learning algorithms [34] in prediction. The basic principle of SVR is as follows:

Define the output variable as:

$$f(x) = w\phi(x) + b \tag{12}$$

where w is a vector of weights. $\phi(x)$ is a nonlinear function that maps x from the input space to a higher-dimensional space. b is deviation.

To find w and b, create a minimization function and compute it:

$$min\delta = \left[\frac{1}{2} \parallel w \parallel^2 + C\sum_{i=1}^{l} (\zeta_i + \zeta_i^*)\right] \tag{13}$$

where δ is the minimization objective function. C is the penalty factor. ζ_i, ζ_i^* are the relaxation variables for the upper and lower boundaries of the i-th sample.

Define ε as the insensitive loss factor. y_i is the output value of the i-th sample. There are ζ_i, ζ_i^*, y_i, ε, and w_i and b to be satisfied:

$$\begin{cases} y_i - w_i - b \leqslant \varepsilon + \zeta_i \\ w_i + b - y_i \leqslant \varepsilon + \zeta_i^* \\ \zeta_i, \zeta_i^* \geqslant 0 \end{cases} \tag{14}$$

By introducing the Lagrange multipliers α_i^* and α, and solving the quadratic planning problem, the regression function is obtained.

$$f(x) = \sum_{i=1}^{n} (\alpha_i^* - \alpha_i) K(x_i, x_j) + b \tag{15}$$

where $K(x_i, x_j)$ is the kernel function. x_i and x_j represent the input vectors of the kernel function. x_i is the input variable in the training set and x_j is the input variable in the test set.

2.5. Deep-Learning Differentiation Models with Double Noise Reduction

Based on SSA, ICEEMDAN, SVR, and GRU neural networks, hybrid models of SSA-ICEEMDAN-SVR-GRU are proposed. The process of constructing the model is shown in Figure 2. The descriptions of the details are given below:

(1) Use SSA to decompose and reconstruct the original data, extract the effective trend information, and discard the noise part. The SSA window length is set to seven, with bus 1 selecting the first five principal component reconstruction data and bus 2 selecting the first three principal component reconstruction data.

(2) Use ICEEMDAN to decompose the data after the SSA noise reduction into subsequences with different complexities to reduce the influence of noise still existing in the data. Add the standard deviation of noise of 0.45 to ICEEMDAN for 1000 times, and the maximum number of iterations is allowed to be 40,000.

(3) Using the complexity of the sample entropy operator sequences, and using 1 as the cutoff point, the subsequences are divided into high-frequency ones and low-frequency ones.

(4) Vehicle speed, engine speed, torque percentage, instantaneous fuel consumption, and gas pedal opening are used as inputs to the sub-model, and the ICEEMDAN decomposed subseries are used as outputs. Model and predict the high-frequency subsequences by GRU. Predict the low-frequency subsequences by SVR. Since the optimal hyperparameters of each sub-model are different, the optimal hyperparameters of each sub-model are obtained by a grid search. The hyperparameters of grid search for the GRU model include the number of hidden layers, number of neurons in hidden layers, number of iterations, and batch size. The hyperparameters of grid search for the SVR model include learning rate, kernel function, number of iterations, and penalty factor. Obtain the final results by integrating the prediction results of the two models.

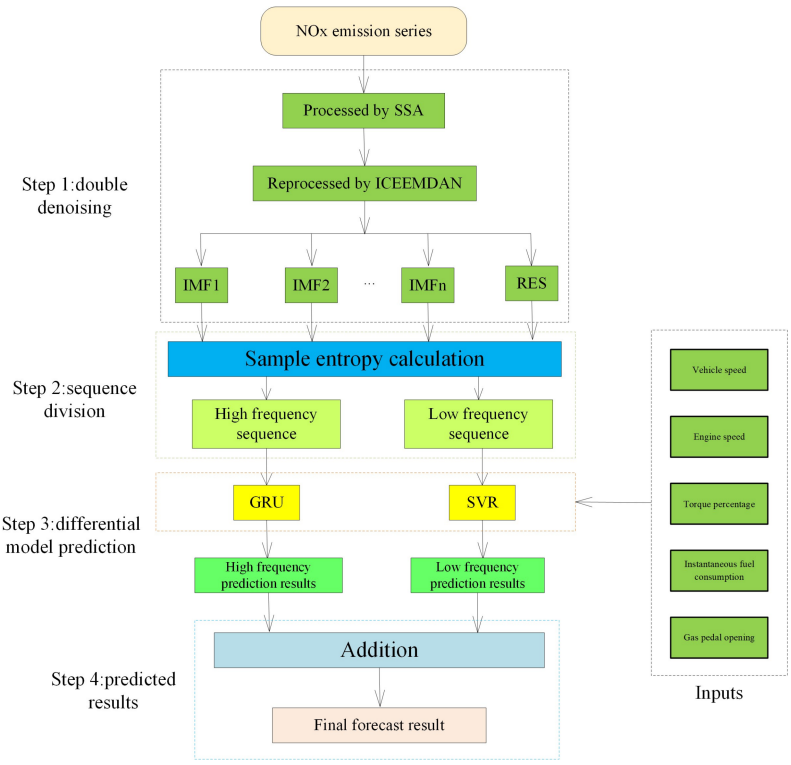

Figure 2. Flow chart of SSA-ICEEMDAN-SVR-GRU models.

In order to test the abilities of SSA-ICEEMDAN-SVR-GRU models to predict the NO_x emissions of diesel vehicles in actual roads, we compare the performance of 12 different

prediction models, including SVR models, LSTM models, GRU models, SSA-SVR models, SSA-LSTM models, SSA-GRU models, ICEEMDAN-SVR models, ICEEMDAN-LSTM models, ICEEMDAN-GRU models, RF (Random Forest) models, and Bayes network models.

3. Case Study

3.1. Data Sources

The data of this study comes from the vehicle exhaust online monitoring platform, which uses the GPRS (General Packet Radio Service) to monitor the real-time exhaust emission of the vehicle when driving on the actual road. The terminal equipment includes a nitrogen oxide sensor, OBD (On-Board Diagnostic) data reader, and wireless data transmission unit. The NO_x sensor is an electrochemical sensor that directly measures the amount of NO_x emissions per second. Through strict management and control, collect and manage the data information of exhaust monitoring parameters and the basic information of vehicles. The data collected by the platform has the characteristics of standardization, authenticity, and accuracy. The basic engine parameters for the two buses are given in Table 2.

Table 2. Basic engine parameters of the two buses.

Parameter	Bus 1	Bus 2
Engine Power	213 kw	206 kw
Air intake System	Turbocharged inter-cooled	Turbocharged inter-cooled
Type	6-cylinder, in-line, electrical control systems	6-cylinder, in-line, water-cooled
Displacement	8.9 L	8.4 L
Maximum Torque (N.m)	1050	1100
Emission Standards	EU IV	EU IV
Rated Speed (rpm)	2100	2200

The experimental data were selected according to the method of Günther et al. [35]. The data acquired by the monitoring platform were divided into individual micro-travels. Micro-travel is defined as the travel between two stops starting at speed zero and ending at speed zero. These stops include bus stops, traffic light sections, and stops due to heavy traffic.

For buses, the selected samples include the data for all the working conditions of idle speed, acceleration, constant speed, deceleration, and stop. The main parameters collected include vehicle speed, engine speed, torque percentage, instantaneous fuel consumption, accelerator pedal opening, and NO_x concentration. By modeling the collected real-time data, the transient emission prediction of NO_x concentration for diesel vehicles is realized.

3.2. Evaluation Indexes

In this paper, root mean square error (RMSE) [36], determination coefficient (R^2) [37], mean absolute error (*MAE*) [36], and normalized root mean squared error (NRMSE) [38] are used to evaluate the performance of the model. The calculation formula is as follows:

$$\mathrm{RMSE} = \sqrt{\frac{1}{n}\sum_{i=1}^{n}(\hat{y}_i - y_i)^2} \tag{16}$$

$$R^2 = 1 - \frac{\sum(y - \hat{y})^2}{\sum(y - \overline{y})^2} \tag{17}$$

$$MAE = \frac{1}{n}\sum_{i=1}^{n}|\hat{y}_i - y_i| \tag{18}$$

$$\mathrm{NRMSE} = \frac{RMSE}{y_{max} - y_{min}} \times 100 \tag{19}$$

here, y is the experimental value, $\hat{y}$ is the predicted value of the model, $\overline{y}$ is the average value of the measured value, y_{max} is the maximum value of NO_x concentration, and y_{min} is the minimum value of NO_x concentration.

3.3. Data Processing Analysis

In this part, the main theories and algorithms are introduced in detail, including the SSA algorithm, ICEEMDAN algorithm, GRU network, and SVR machine learning algorithm. Among them, GRU and SVR models are completed by Python 3.6, and data processing algorithms, including SSA, and ICEEMDAN are completed by MATLAB 2019b.

3.3.1. Singular Spectrum Noise Reduction

In the process of SSA noise reduction, the window length L and the number of reconstructed principal components m are determined. Generally, let $L < \frac{N}{2}$, where N is the length of the noise-reduction sequence, and the proportion of the sequence period [38]. Since there are no obvious periodic changes in the actual driving process of diesel buses, it is more appropriate to set the window length L as seven after the test. The number of principal components m is very important for reconstructions and noise reductions, the value of which is usually set based on the contribution rate of each principal component eigenvalue. Generally, the contribution of the noise component is very small. The component characteristics of the two buses are shown in Figure 3. It can be seen from Figure 3 that the first two components are significantly larger than the rest, indicating that they have more information content. Table 3 shows the performance results of SSA-SVR models when m takes different values. It is found from Table 3 that bus 1 has the best result when m = 5, which indicates that the data after component 5 is the noise components that should be removed, and the information component before component 5 should be retained. From Table 3, it is found that bus 2 has the best result when m = 3, which indicates that the data after component 3 contains noises that are directly so the information of the first three components is retained. Figure 4 shows the NO_x emission sequence results after the SSA treatment.

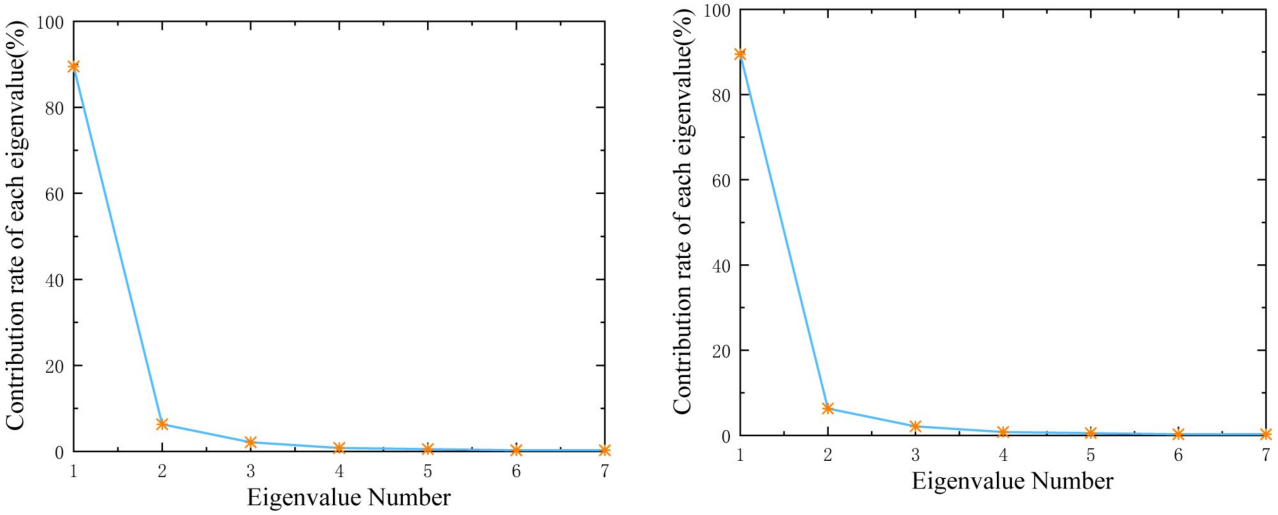

Figure 3. Component characteristics of two buses ((**a**) bus, (**b**) bus 2).

Table 3. Comparison of SSA-SVR results with different m values.

	RMSE (ppm)		R^2		MAE (ppm)	
m	**Bus 1**	**Bus 2**	**Bus 1**	**Bus 2**	**Bus 1**	**Bus 2**
3	97.512	90.112	0.917	0.897	54.967	51.897
4	97.139	92.692	0.923	0.896	55.033	52.998
5	96.982	91.892	0.925	0.899	55.015	52.392
6	98.939	90.934	0.922	0.902	55.739	52.401
Unused SSA	112.458	107.485	0.901	0.865	60.553	57.861

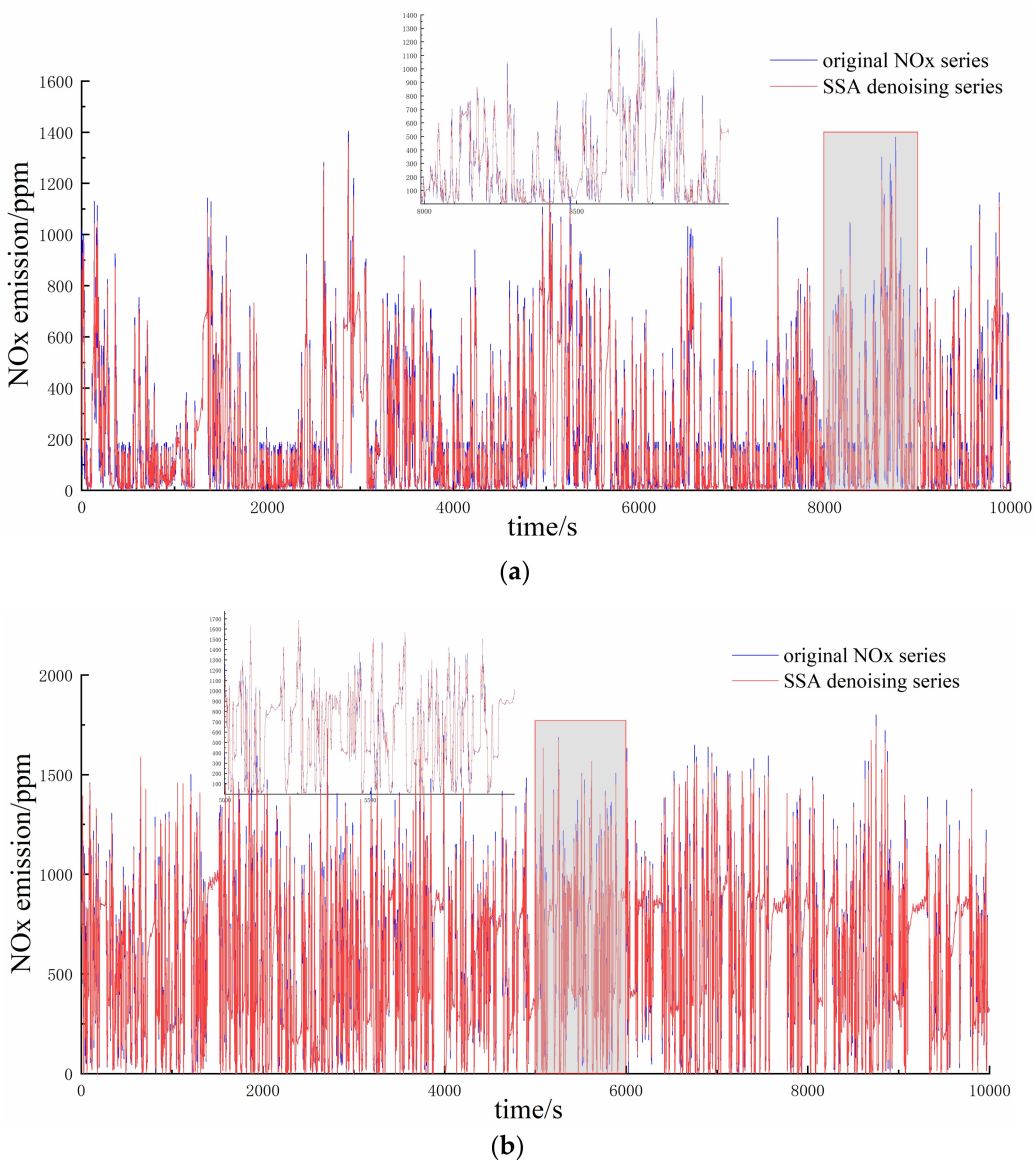

Figure 4. Comparison of NO_x concentration sequence before and after SSA treatment ((**a**) bus 1, (**b**) bus 2).

3.3.2. ICEEMDAN Decomposition Sequence

After the noise of the original NO_x concentration data is reduced by SSA, use ICEEMDAN to decompose the data and obtain the subsequences of two buses. Then add the standard deviation of noise of 0.45 to ICEEMDAN for 1000 times, and the maximum number of iterations is allowed to be 40,000, which fully avoided the influence of noises on the results. The decomposition results of the two buses are shown in Figure 5. The fluctuation

frequency of the subsequence gradually becomes stable with the increase of decomposition times until there are residual quantities of a single trend. Bus 1 is decomposed into 13 IMFs and 1 RES, bus 2 is decomposed into 12 IMFs and 1 RES.

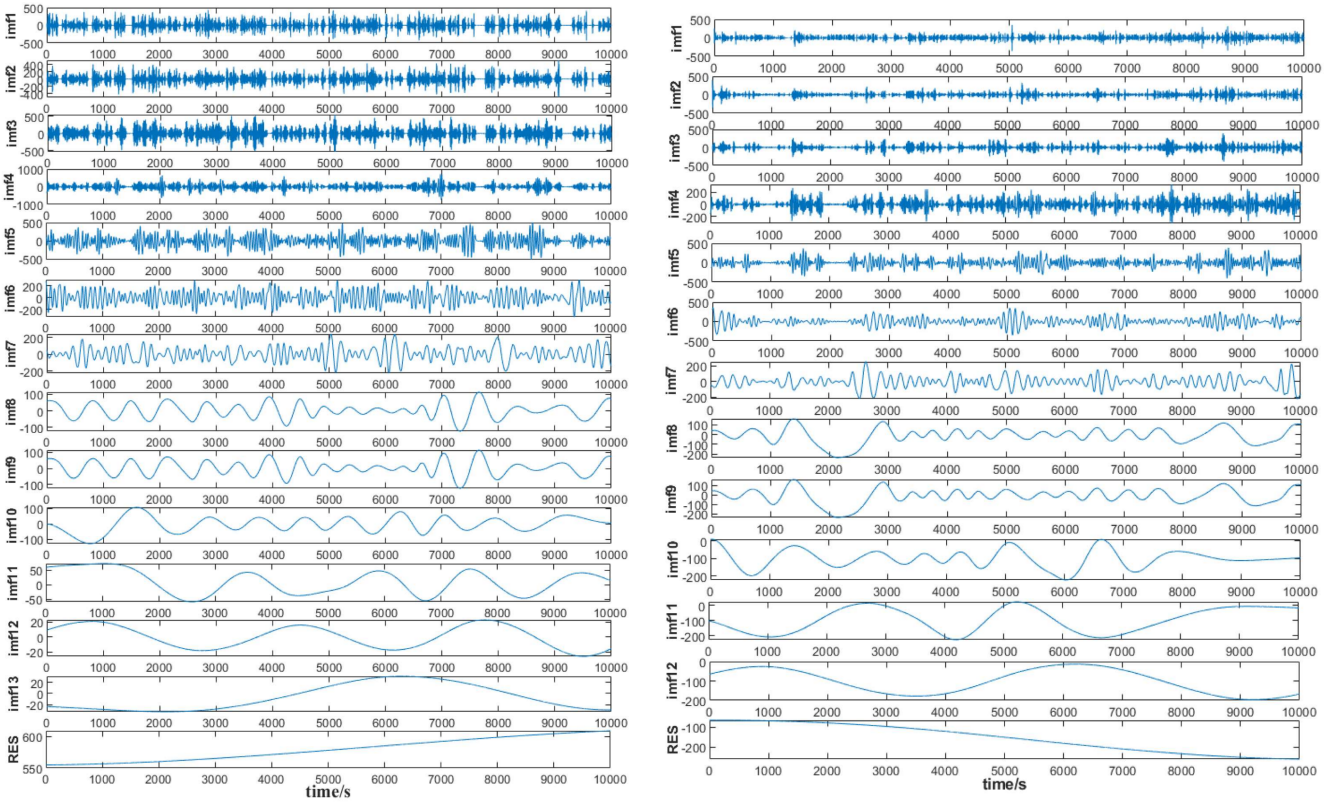

Figure 5. Series results of ICEEMDAN decomposing the NO_x emission ((**a**) bus 1, (**b**) bus 2).

3.3.3. Calculation of Sub-Sequence Complexity

In order to reduce the computational complexity of the GRU neural network and avoid overfitting situations, calculate the complexity of the NO_x concentration series by the sample entropy. The sample entropy can be used to evaluate the repetition of the waveform before and after or frequencies. The higher the entropy, the greater the frequency change in the waveform, and the more repetitive the waveform; the lower the entropy, the smaller the frequency change in the waveform, and the less repetitive the waveform. According to the complexity of subsequences, divide the subsequences into high-frequency ones and low-frequency ones. Use GRU neural network to predict high frequency, and use SVR to predict low frequency. The calculation results of sample entropy of two bus NO_x emission subsequences are shown in Table 4.

Looking at Figure 5 and Table 4, the greater the sample entropy, the more obvious the frequency change of subsequence, and the higher the complexity. When the sample entropy is lower than 1, the fluctuation of sequence data is more gentle. Therefore, this paper takes the sample entropy value equal to 1 as the division standard of high-frequency and low-frequency sequences. IMF1 to IMF6 of bus 1 are predicted using GRU neural network, and IMF7 to IMF13, including RES, are predicted by SVR; IMF1 to IMF5 of bus 2 are predicted using GRU neural networks, and IMF6 to IMF12, including RES, are predicted by SVR.

Table 4. Sample entropy calculations for each subseries.

Bus 1		Bus 2	
Sequence	**Sample Entropy**	**Sequence**	**Sample Entropy**
IFM1	2.359	IFM1	1.866
IFM2	2.114	IFM2	1.741
IFM3	1.407	IFM3	1.959
IFM4	1.372	IFM4	1.681
IFM5	1.586	IFM5	1.451
IFM6	1.019	IFM6	0.758
IFM7	0.729	IFM7	0.682
IFM8	0.554	IFM8	0.533
IFM9	0.451	IFM9	0.467
IFM10	0.397	IFM10	0.305
IFM11	0.189	IFM11	0.185
IFM12	0.426	IFM12	0.018
IFM13	0.158	RES	0.001
RES	0.004		

3.3.4. Analysis of the Prediction Results of Each Sub-Sequence by GRU and SVR

For the subsequences decomposed by ICEEMDAN, use GRU and SVR models to predict the high-frequency and low-frequency subsequences respectively. Observe the learning situation of the subsequences. For NO_x emission of the two buses, the multi-index evaluation results of each subsequence prediction model are given in Table 5.

Table 5. Multi-index evaluation results of the subsequence prediction model for NO_x concentration.

	Bus 1					Bus 2				
Sequence	**Model**	**RMSE (ppm)**	R^2	**MAE (ppm)**	**Time (s)**	**Model**	**RMSE (ppm)**	R^2	**MAE (ppm)**	**Time (s)**
IMF1	GRU model	43.304	0.620	25.037	163	GRU model	34.168	0.510	20.837	158
IMF2		17.456	0.955	10.711	162		13.381	0.944	9.030	157
IMF3		3.797	0.999	2.590	162		3.603	0.998	2.648	157
IMF4		2.035	0.999	1.596	162		1.236	0.999	0.935	157
IMF5		0.894	0.999	0.657	162		0.761	0.999	0.564	157
IMF6		0.889	0.999	0.651	162		1.437	0.999	0.992	5
IMF7		0.707	0.999	0.533	5		1.200	0.999	0.745	5
IMF8		1.739	0.999	1.335	5		1.063	0.999	0.628	4
IMF9	SVR model	0.297	0.999	0.216	4	SVR model	0.846	0.999	0.662	4
IMF10		0.503	0.999	0.434	4		0.128	0.999	0.081	4
IMF11		0.226	0.999	0.185	4		0.385	0.999	0.198	4
IMF12		0.242	0.999	0.194	4		0.194	0.999	0.156	3
IMF13		0.053	0.999	0.035	3		NA *	NA	NA	NA
RES		0.406	0.999	0.358	3		0.241	0.999	0.211	3

* means no data.

In the experiment, the high-frequency sequence IMF1 of bus 1 and bus 2 is complex. According to the GRU model, the value for the two buses R^2 are 0.620 and 0.510 respectively, which indicates that the noise or outliers may be decomposed into IMF1 during the decomposition process, which affects the prediction effects of the models. However, with the increase of decomposition times, the noise data in the subsequence is gradually reduced, and the prediction stability of the model is significantly enhanced, with a R^2 which is close to 1, indicating that the predicted and actual values of the subsequence are very close, and the prediction effects are excellent. In the low-frequency sequence, the SVR model also shows good effects, and the value of R^2 is close to 1, which shows that in the low-frequency sequence, SVR can replace GRU, and the calculation time of the SVR model is much lower

than that of GRU models. Therefore, use the SVR model to reduce the prediction time in low-frequency sequences, but the prediction performance of the model is still stable.

4. Results and Discussion

In order to verify the prediction performance of the multiple noise-reduction deep-learning differentiated model SSA-ICEEMDAN-SVR-GRU proposed in this paper, a comparative analysis was carried out. First, compare the model with five single models of GRU, LSTM, SVR, Bayes, and RF without noise reductions; then compare the model with GRU, LSTM, and SVR that have undergone SSA one-step noise reduction; in addition, ICEEMDAN-GRU, ICEEMDAN-LSTM, and ICEEMDAN-SVR models are added for comparison, involving a total of 12 different models for comparison. Table 6 lists the multi-index evaluation results of two buses using different models.

Table 6. Comparison of multi-index forecast results.

Model	RMSE (ppm)		R^2		MAE (ppm)		NRMSE (%)	
	Bus 1	Bus 2	Bus 1	Bus 2	Bus 1	Bus 2	Bus 1	Bus 2
SVR	112.630	97.609	0.901	0.889	60.284	49.006	6.458	7.716
Bayes	125.557	95.229	0.877	0.885	76.681	61.382	7.167	7.528
RF	113.412	94.232	0.899	0.888	65.928	56.859	6.479	7.449
LSTM	104.178	99.938	0.915	0.883	55.575	56.616	5.974	7.900
GRU	103.032	98.723	0.917	0.886	55.535	54.331	5.908	7.804
SSA-SVR	97.079	83.442	0.924	0.912	54.816	45.253	5.566	6.596
SSA-LSTM	90.449	80.623	0.934	0.918	51.719	48.611	5.186	6.373
SSA-GRU	88.915	80.832	0.937	0.917	49.922	48.166	5.098	6.390
ICEEMDAN -SVR	77.607	60.868	0.953	0.957	46.193	39.647	4.450	4.812
ICEEMDAN -LSTM	68.217	55.702	0.964	0.964	43.071	35.91	3.912	4.403
ICEEMDAN -GRU	69.371	56.824	0.962	0.962	43.832	36.705	3.978	4.492
SSA-ICEEMDAN-SVR-GRU	46.904	46.782	0.983	0.974	30.735	30.859	2.689	3.698

4.1. Comparative Analysis of Single Models

It is not possible to achieve ideal results in the transient NO_x emission. Taking the transient NO_x emission prediction results of bus 2 as an example, the RMSE, MAE, and R^2 of the SSA-ICEEMDAN-SVR-GRU models are increased by 52.613, 43.202, and 9.932% respectively compared to the GRU models. Compared with the random forest model, the RMSE, MAE, and R^2 of the SSA-ICEEMDAN-SVR-GRU model are improved by 50.354, 45.727, and 9.685%, respectively.

In order to further analyze and verify the predictive ability of the SSA-ICEEMDAN-SVR-GRU models on the instantaneous emission of NO_x from two buses, Figure 6 shows the comparison results for the five single models of Bayes, RF, SVR, LSTM, and GRU. Combining Table 6, it can be found that the predictive ability of single models is limited and cannot accurately capture the significant characteristics of transient NO_x concentration emissions, and the prediction error is relatively large. Single models can predict the overall trend of changes in NO_x transient emissions, but there are huge gaps between the predicted result and the actual value. The main reason for this result is that in the actual road operation of diesel vehicles, the road conditions are complex and changeable. The driver needs to adjust the fuel supply and emergency braking constantly. The engine presents an irregular and rapid change state, which directly affects diesel combustion and NO_x emissions. It is difficult for single models to capture the transient emission law of NO_x, and it is impossible to model and predict accurately.

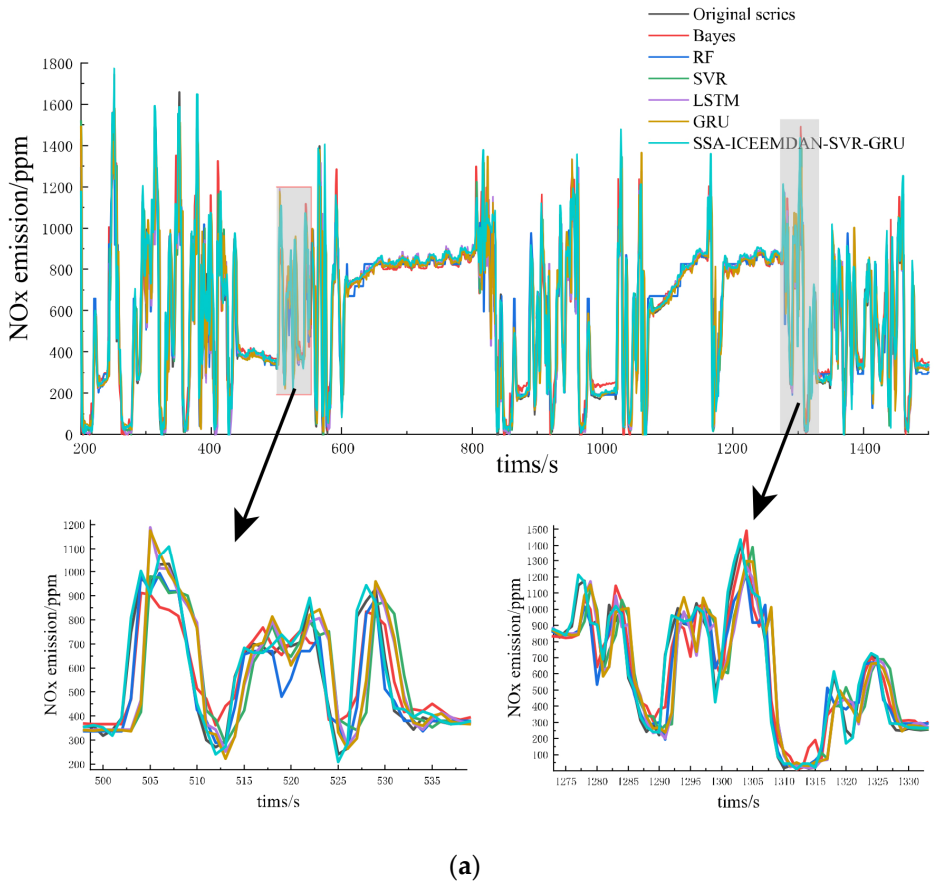

(**a**)

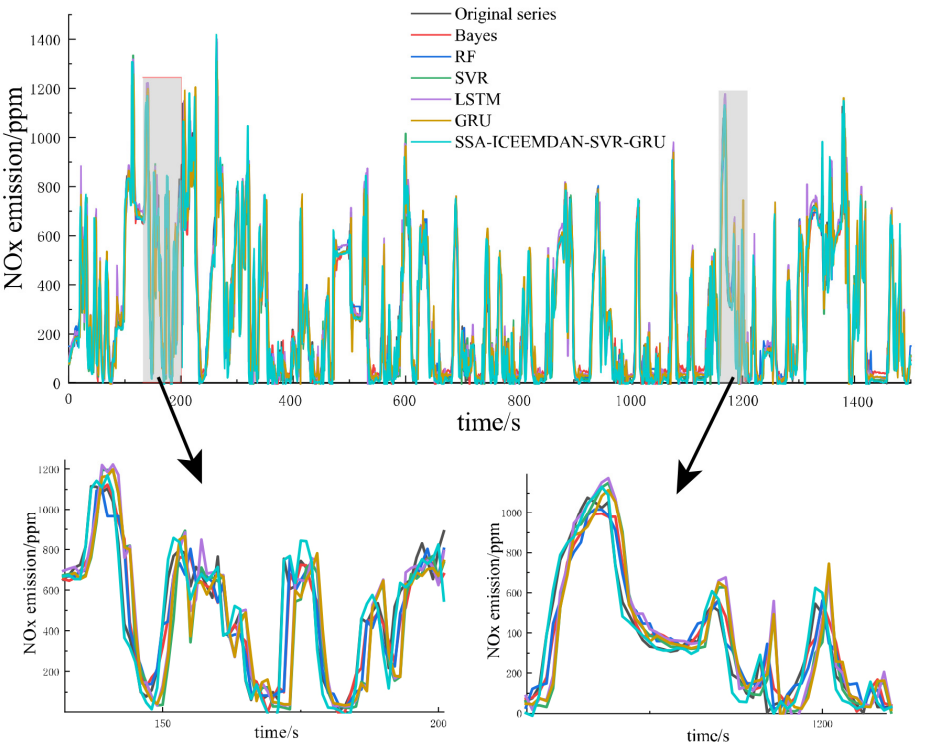

(**b**)

Figure 6. Comparison of the prediction of NO_x emissions from two buses using a single model ((**a**) single model comparison results of bus 1, (**b**) single model comparison results of bus 2).

4.2. Comparative Analysis of SSA Single Treatment Results

After the original data is processed by SSA noise reduction, the prediction accuracy is significantly higher than that of a single model. For example, in bus 2, the RMSE, MAE, and R^2 of SSA-GRU are improved by 18.122, 11.347, and 3.500%, respectively. However, compared with the SSA-ICEEMDAN-SVR-GRU model, satisfactory prediction results are still not achieved. In the transient NO_x emission prediction results of bus 2, the SSA-ICEEMDAN-SVR-GRU model is better than the RMSE of the SSA-GRU model, in which the values of MAE and R^2 increased by 42.124, 35.932, and 6.181% respectively.

Figure 7 shows the modeling results after processing the transient NO_x emission results of two buses using singular spectrum analysis. Through comparative analysis of Figures 6 and 7, it can be found that the noise after the original sequence is reduced by SSA and the NO_x sequence shows a more obvious trend. The regularity of the NO_x transient sequence can be found more easily by using a machine learning model, and the stability and generalization of the model can be enhanced. By comparing the first mock exam with the SSA model, the R^2 of SVR, LSTM, and GRU increased by 2.587, 3.964, and 3.533% respectively, which means that SSA can enhance the interpretability and prediction ability of the model. Table 3 shows the influence of different values of SSA-SVR model m on the prediction results. In the process of SSA noise reduction, if the m value is too large, the noise in the NO_x emission sequence may not be filtered completely, which will directly affect the basic information of the NO_x emission sequence; if the value of m is too small, the correct, and useful information in the original sequence will be filtered out. Therefore, selecting an appropriate m value to filter the transient emission data of NO_x can improve the data quality, reduce the influence of random interference, and enhance the prediction accuracy and stability of the model. The experimental results show that SSA noise reduction is very helpful to extract useful information from the original NO_x sequence and improve the prediction accuracy of NO_x transient emission.

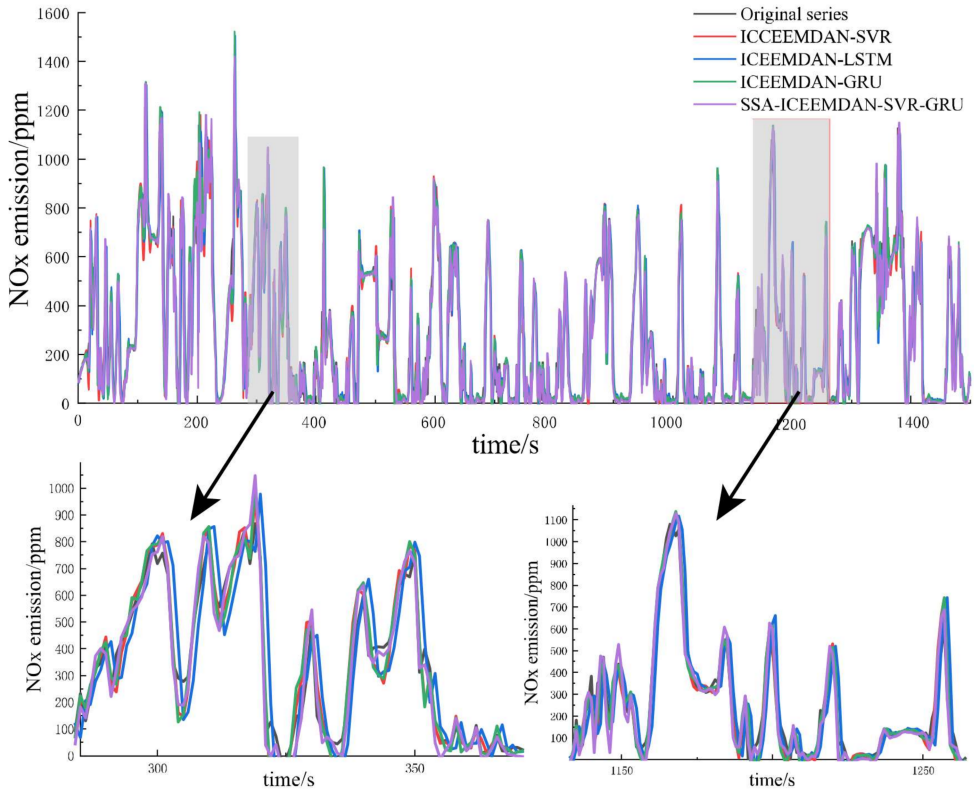

(**a**)

Figure 7. *Cont.*

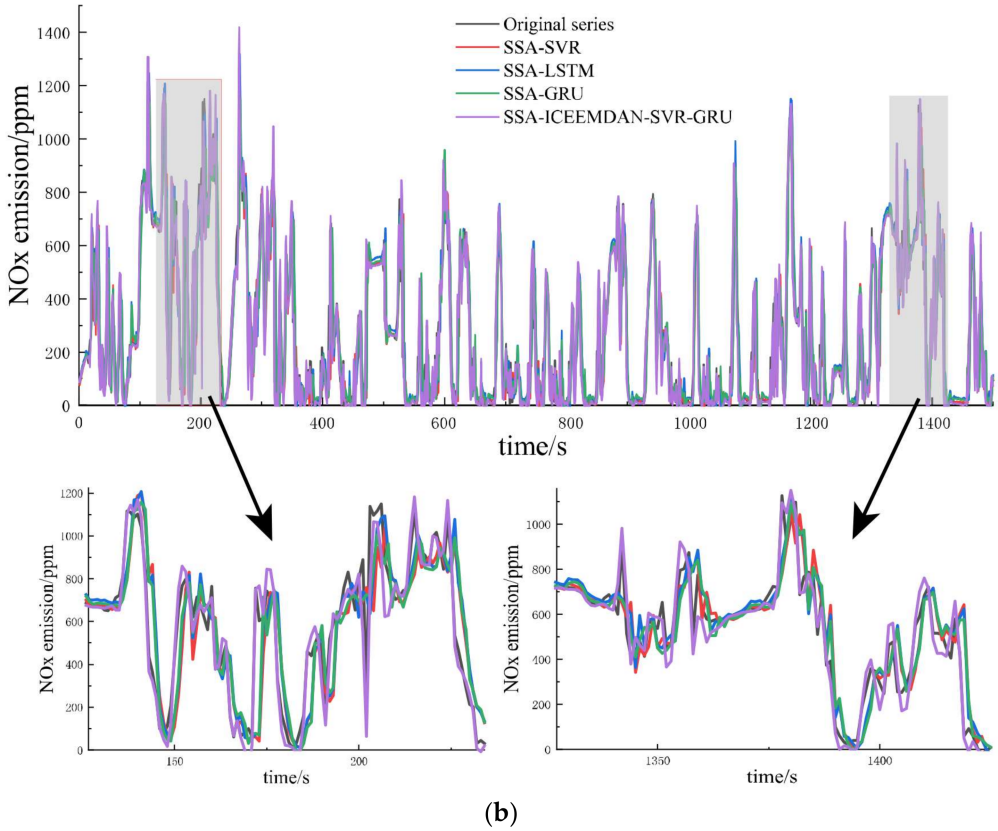

Figure 7. Comparison of prediction results of NO_x emission of two buses using SSA ((**a**) comparison of noise-reduction prediction results of bus1 SSA, (**b**) comparison of noise-reduction prediction results of bus 2 SSA).

4.3. Comparative Analysis of Single Treatment Results of ICEEMDAN

The original data is decomposed by ICEEMDAN and then modeled. The prediction accuracy and stability are significantly higher than the single model and the SSA noise reduction processing model. For example, for bus 2, the RMSE, MAE, and R^2 of the ICEEMDAN-GRU model are improved by 42.44%, 32.442, and 8.58%, respectively, compared with the single model GRU. The RMSE, MAE, and R^2 of the ICEEMDAN-GRU model are increased by 29.701, 23.795, and 4.907%, respectively, compared to the SSA-GRU noise-reduction model SSA-GRU. Through the comparison of the above two groups, it is found that the ICEEMDAN decomposition has a better noise-reduction effect on nonlinear and unstable data, and it is easier to mine the internal information and characteristics of the data. However, the dual noise-reduction SSA-ICEEMDAN-SVR-GRU model increased the RMSE, MAE, and R^2 of ICCEMDAN-GRU by 17.672, 15.927, and 1.248%, respectively.

Figure 8 shows the comparison results of modeling and comparison of the original NO_x emission sequences of two buses after ICEEMDAN processing. Figures 6–8 are compared and analyzed. The original sequence of NO_x emissions is processed by ICEEMDAN and then modeled and predicted. The predicted result is closer to the experimental value, and more accurate prediction results can be obtained under high-load and high-speed conditions of diesel vehicles. Combining Table 6, it is found that the prediction performance of the model processed by ICEEMDAN is higher than that of SSA noise reduction. For example, in the GRU model of bus 2, the RMSE of the SSA-GRU model is 18.122% higher than that of the GRU model, and the ICEEMDAN-GRU is 42.441% higher than the GRU. This improvement is mainly due to the fact that ICEEMDAN decomposes the transient NO_x emission sequence into multiple subsequences with different frequency fluctuations. From Table 4, it is found that these subsequences have lower sample entropy, that is, they

have lower sample entropy. The complexity of the model can better capture the changing law of the sequence, thereby improving the predictive ability.

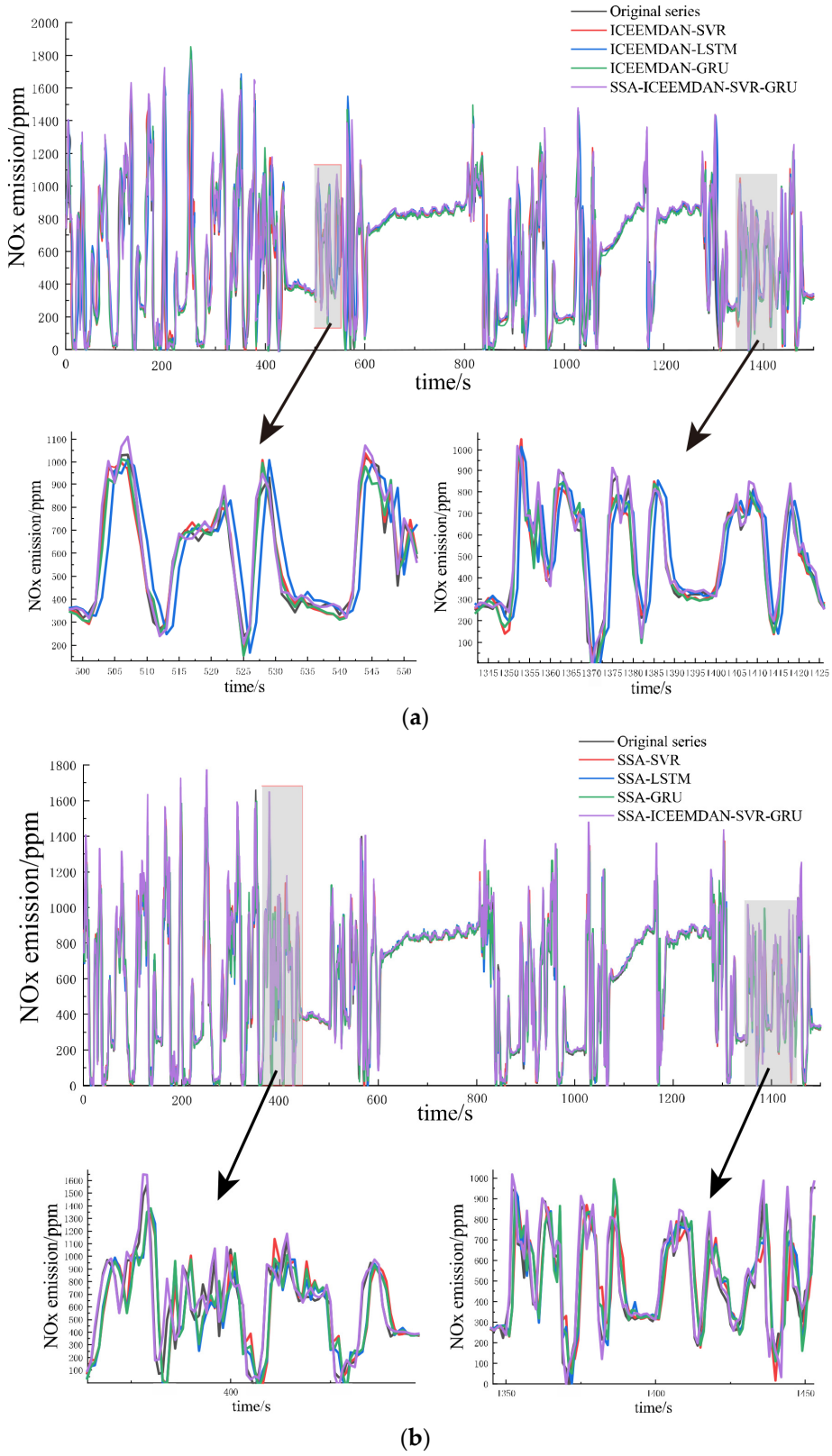

Figure 8. Comparison of prediction results of NO_x emission from two buses using ICEEMDAN ((**a**) comparison of ICEEMDAN processing and prediction results of bus 1, (**b**) comparison of ICEEMDAN processing and prediction results of bus 2).

The comparison of the dual noise-reduction differential model SSA-ICEEMDAN-SVR-GRU with the single model and single-processing model shows that the prediction accuracy of the model proposed in this paper is higher than other models. Among them, a single model has the worst performance. This is because the originally collected NO_x emission sequence contains a lot of noise and a variety of fluctuating frequencies. A single model cannot learn its laws well and accurately. After the noise of the original NO_x emission sequence is reduced by SSA, the noise in the sequence is significantly reduced, the model can better capture the sequence information, and the accuracy of the model is improved. The original data is directly processed by ICEEMDAN, which can obtain better prediction results. However, because ICEEMDAN directly decomposes the original sequence, the subsequence is less complex than the original sequence, and the sampling results of different frequencies are distributed in different subsequences, which is easier to find than the law but does not filter the noise, so the prediction accuracy is still insufficient. After the noise of the original sequence is reduced by SSA, ICEEMDAN is used to decompose, and the accuracy of the model is further improved. At the same time, the complexity of subsequences is analyzed through sample entropy, and SVR is used to replace low-complexity subsequences, which reduces the calculation cost and prediction time while maintaining model stability and prediction accuracy. Therefore, the SSA-ICEEMDAN-SVR-GRU model proposed in this paper is a prediction method with excellent performance. By comparing different models, using SSA to reduce the noise of the transient NO_x emissions for diesel vehicles, and ICEEMDAN decomposition can effectively improve the prediction accuracy of the model.

5. Conclusions

This research proposes a differential model SSA-ICEEDMAN-SVR-GRU with dual noise reduction to improve the prediction of transient NO_x emissions of diesel vehicles. In the proposed SSA-ICEEDMAN-SVR-GRU model, SSA is used for noise reduction, ICEEMDAN is used to decompose the data, and sample entropy is used to calculate the subseries complexity, using a differentiation model depending on the complexity. The proposed model is validated with data from two buses and compared with five single models, three SSA processing models, and three ICEEMDAN processing models. Based on the comparison of three sets of experiments, the following conclusions are drawn:

(1) After noise reduction by SSA, the prediction model is established. The accuracy is higher than that of a single model. It shows that SSA can remove the outliers in the original sequence. It also shows that noise has a great influence on the prediction results of NO_x transient emissions of diesel vehicles.
(2) Using ICEEMDAN to process the original data and then modeling, the prediction accuracy is significantly improved, indicating that ICEEMDAN's decomposition method can effectively extract the trend law and useful information of the original sequence, which helps the model learn its internal laws and improve the performance of the model.
(3) After comprehensively considering SSA noise reduction and ICEEDAN decomposition, the combined model SSA-ICEEMDAN-SVR-GRU has the best prediction performance. The results show that double noise reduction has better prediction performance than the single-processing method in improving the accuracy of transient NO_x emission prediction.
(4) The use of SVR in the low-frequency sequence instead of the GRU model with higher computational cost can reduce the prediction time and maintain the prediction performance of the model.

Overall, the SSA-ICEEMDAN-SVR-GRU model proposed in this paper helps to analyze the diesel vehicle's NO_x emissions on actual roads, replacing physical NO_x emissions sensors with virtual NO_x emissions sensors, etc., to provide transient NO_x emissions for diesel vehicles A new method.

The model proposed in this paper shows excellent performance in the prediction of NO_x transient emissions from diesel vehicles. In the future, we will consider the method proposed in this paper to predict other pollutants of diesel vehicles, such as HC, PM, CO, etc., to reduce the cost of experimental measurement and experimental complexity.

Author Contributions: Data curation, Y.W. and L.Z.; writing—original draft preparation, Y.Y.; writing—review and editing, J.L.;project administration, C.H. All authors have read and agreed to the published version of the manuscript.

Funding: This research was funded by National Natural Science Foundation of China grant number 51968065 and Yunnan Provincial high level talent support project grant number YNWR-QNBJ-2018-066, YNQR-CYRC-2019-001.

Institutional Review Board Statement: Not applicable.

Informed Consent Statement: Not applicable.

Data Availability Statement: The data used to support the findings of this study are available from the corresponding author upon request.

Conflicts of Interest: All authors disclosed no relevant relationships.

References

1. Ministry of Ecology and Environment of the People's Republic of China. *China Mobile Source Environmental Management Annual Report*; China Ministry of Ecology and Environment: Beijing, China, 2020; Volume 1, pp. 1–7.
2. Giakoumis, E.; Alafouzos, A. Study of diesel engine performance and emissions during a Transient Cycle applying an engine mapping-based methodology. *Appl. Energy* **2010**, *87*, 1358–1365. [CrossRef]
3. Wang, G.; Awad, O.I.; Liu, S.; Shuai, S.; Wang, Z. NO_x emissions prediction based on mutual information and back propagation neural network using correlation quantitative analysis. *Energy* **2020**, *198*, 117286. [CrossRef]
4. Abulut, M.; Ayyildiz, M.; Sardemir, S. Prediction of performance, combustion and emission characteristics for a CI engine at varying injection pressures. *Energy* **2020**, *197*, 117257. [CrossRef]
5. Lotfan, S.; Ghiasi, R.A.; Fallah, M.; Sadeghi, M. ANN-based modeling and reducing dual-fuel engine's challenging emissions by multi-objective evolutionary algorithm NSGA-II. *Appl. Energy* **2016**, *175*, 91–99. [CrossRef]
6. Duan, H.; Huang, Y.; Mehra, R.K.; Song, P.; Ma, F. Study on influencing factors of prediction accuracy of support vector machine (SVM) model for NO_x emission of a hydrogen enriched compressed natural gas engine. *Fuel* **2018**, *234*, 954–964. [CrossRef]
7. Kumbala, B.R. *Predictive Maintenance of NOx Sensor Using Deep Learning: Time Series Prediction with Encoder-Decoder LSTM*; Blekinge Tekniska Hogskola: Karlskrona, Sweden, 2019.
8. Maurya, R.K.; Mishra, P. Parametric investigation on combustion and emissions characteristics of a dual fuel (natural gas port injection and diesel pilot injection) engine using 0-D SRM and 3D CFD approach. *Fuel* **2017**, *210*, 900–913. [CrossRef]
9. Provataris, S.A.; Savva, N.S.; Chountalas, T.D.; Hountalas, T. Prediction of NO_x emissions for high speed DI Diesel engines using a semi-empirical, two-zone model. *Energy Convers. Manag.* **2017**, *153*, 659–670. [CrossRef]
10. Hsieh, M.-F.; Wang, J. NO and NO_2 concentration modeling and observer-based estimation across a diesel engine aftertreatment system. *J. Dyn. Syst. Meas. Control* **2011**, *133*, 041005. [CrossRef]
11. Liu, Y.; Midkiff, K.; Bell, S. Development of a multizone model for direct injection diesel combustion. *Int. J. Engine Res.* **2004**, *5*, 71–81. [CrossRef]
12. Panis, L.I.; Broekx, S.; Liu, R. Modelling instantaneous traffic emission and the influence of traffic speed limits. *Sci. Total Environ.* **2006**, *371*, 270–285. [CrossRef]
13. Smit, R.; Ntziachristos, L.; Boulter, P. Validation of road vehicle and traffic emission models–A review and meta-analysis. *Atmos. Environ.* **2010**, *44*, 2943–2953. [CrossRef]
14. Altuğ, K.B.; Küçük, S.E. Predicting Tailpipe NO_x Emission using Supervised Learning Algorithms. In Proceedings of the 2019 3rd International Symposium on Multidisciplinary Studies and Innovative Technologies (ISMSIT), Ankara, Turkey, 11–13 October 2019.
15. Liu, B.; Hu, J.; Yan, F.; Turkson, F.; Lin, F. A novel optimal support vector machine ensemble model for NO_x emissions prediction of a diesel engine. *Measurement* **2016**, *92*, 183–192. [CrossRef]
16. Domínguez-Sáez, A.; Rattá, G.A.; Barrios, C.C. Prediction of exhaust emission in transient conditions of a diesel engine fueled with animal fat using Artificial Neural Network and Symbolic Regression. *Energy* **2018**, *149*, 675–683. [CrossRef]
17. Lavda, F.; Ramapuram, J.; Gregorova, M.; Alexandors, K. Continual Classification Learning Using Generative Models. *arXiv* **2018**, arXiv:1810.10612.
18. Shin, S.; Lee, Y.; Kim, M.; Park, J.; Lee, S.; Min, K. Deep neural network model with Bayesian hyperparameter optimization for prediction of NO_x at transient conditions in a diesel engine. *Eng. Appl. Artif. Intell.* **2020**, *94*, 103761. [CrossRef]

19. Bokde, N.; Feijóo, A.; Villanueva, D.; Kulat, K. A Review on Hybrid Empirical Mode Decomposition Models for Wind Speed and Wind Power Prediction. *Energies* **2019**, *12*, 254. [CrossRef]
20. Ma, Z.; Chen, H.; Wang, J.; Yang, X.; Yan, R.; Jia, J.; Xu, W. Application of hybrid model based on double decomposition, error correction and deep learning in short-term wind speed prediction. *Energy Convers. Manag.* **2020**, *205*, 112345. [CrossRef]
21. Tong, C.; Li, J.; Lang, C.; Kong, F.; Niu, J.; Rodrigues, J. An efficient deep model for day-ahead electricity load forecasting with stacked denoising auto-encoders. *J. Parallel Distrib. Comput.* **2018**, *117*, 267–273. [CrossRef]
22. Niu, H.; Xu, K.; Wang, W. A hybrid stock price index forecasting model based on variational mode decomposition and LSTM network. *Appl. Intell.* **2020**, *50*, 4296–4309. [CrossRef]
23. Zhang, X.; Wang, J.; Zhang, K. Short-term electric load forecasting based on singular spectrum analysis and support vector machine optimized by Cuckoo search algorithm. *Electr. Power Syst. Res.* **2017**, *146*, 270–285. [CrossRef]
24. Xiao, L.; Shao, W.; Yu, M.; Ma, J.; Jin, C. Research and application of a hybrid wavelet neural network model with the improved cuckoo search algorithm for electrical power system forecasting. *Appl. Energy* **2017**, *198*, 203–222. [CrossRef]
25. Vautard, R.; Yiou, P.; Ghil, M. Singular-spectrum analysis: A toolkit for short, noisy chaotic signals. *Phys. D Nonlinear Phenom.* **1992**, *58*, 95–126. [CrossRef]
26. Li, T.; Zhou, Y.; Li, X.; Wu, J.; He, T. Forecasting daily crude oil prices using improved CEEMDAN and ridge regression-based predictors. *Energies* **2019**, *12*, 3603. [CrossRef]
27. Colominas, M.A.; Schlotthauer, G.; Torres, M.E. Improved complete ensemble EMD: A suitable tool for biomedical signal processing. *Biomed. Signal Process. Control* **2014**, *14*, 19–29. [CrossRef]
28. Chen, Z.; Li, Y.; Cao, R.; Ali, W.; Liang, H. A New Feature Extraction Method for Ship-Radiated Noise Based on Improved CEEMDAN, Normalized Mutual Information and Multiscale Improved Permutation Entropy. *Entropy* **2019**, *21*, 624. [CrossRef] [PubMed]
29. Hochreiter, S.; Schmidhuber, J. Long Short-Term Memory. *Neural Comput.* **1997**, *9*, 1735–1780. [CrossRef] [PubMed]
30. Dey, R.; Salemt, F.M. Gate-variants of gated recurrent unit (GRU) neural networks. In Proceedings of the 2017 IEEE 60th international midwest symposium on circuits and systems (MWSCAS), Boston, MA, USA, 6–9 August 2017.
31. Agarap, A.F.M. A neural network architecture combining gated recurrent unit (GRU) and support vector machine (SVM) for intrusion detection in network traffic data. In Proceedings of the 2018 10th International Conference on Machine Learning and Computing, Macau, China, 26–28 February 2018.
32. Minh, D.L.; Sadeghi-Niaraki, A.; Huy, H.D.; Min, K.; Hyeonjoon, M. Deep learning approach for short-term stock trends prediction based on two-stream gated recurrent unit network. *IEEE Access* **2018**, *6*, 55392–55404. [CrossRef]
33. Karimipour, A.; Bagherzadeh, S.A.; Taghipour, A.; Abdollahi, A.; Safaei, M. A novel nonlinear regression model of SVR as a substitute for ANN to predict conductivity of MWCNT-CuO/water hybrid nanofluid based on empirical data. *Phys. A Stat. Mech. Appl.* **2019**, *521*, 89–97. [CrossRef]
34. Jalalifar, S.; Masoudi, M.; Abbassi, R.; Garaniya, V.; Ghiji, M.; Salehi, F. A hybrid SVR-PSO model to predict a CFD-based optimised bubbling fluidised bed pyrolysis reactor. *Energy* **2020**, *191*, 116414. [CrossRef]
35. Günther, R.; Wenzel, T.; Wegner, M.; Rettig, R. Big data driven dynamic driving cycle development for busses in urban public transportation. *Transp. Res. Part D Transp. Environ.* **2017**, *51*, 276–289. [CrossRef]
36. Wang, W.; Lu, Y. Analysis of the mean absolute error (MAE) and the root mean square error (RMSE) in assessing rounding model. *IOP Conf. Ser. Mater. Sci. Eng.* **2018**, *324*, 012049. [CrossRef]
37. Nagelkerke, N.J. A note on a general definition of the coefficient of determination. *Biometrika* **1991**, *78*, 691–692. [CrossRef]
38. Stephen, K.D.; Kazemi, A. Improved normalization of time-lapse seismic data using normalized root mean square repeatability data to improve automatic production and seismic history matching in the Nelson field. *Geophys. Prospect.* **2014**, *62*, 1009–1027. [CrossRef]